A stochastic sub-grid viscosity model and wavelet based method for images assimilation

Souleymane Kadri, Etienne Mémin

A stochastic sub-grid viscosity model and wavelet based method for images assimilation

Souleymane Kadri Harouna and Etienne Mémin

Abstract. In this work, we present a wavelet based numerical scheme to discretize the Navier-Stokes equations with location uncertainties [**31**]. This model relies on the decomposition of the flow in terms of a smooth in time resolved component and a highly fluctuating random component. This modeling enables to constitute large-scale dynamical models in which the effect of the unresolved random components is taken into account through the constitution of an anisotropic sub-grid viscosity model without needing any eddy-viscosity assumption. Image data assimilation is used to estimate and optimize the contribution of this stress tensor, directly related to the variance tensor of the unresolved small-scale flow components. This leads to an explicit treatment of the sub-grid viscosity model that enforced the time step limit. Numerical Examples are provided in two space dimension in the case of an inhomogeneous turbulent flow.

Contents

2010 *Mathematics Subject Classification.* 93C20, 93B07.

Key words and phrases. Navier-Stokes, uncertainty modeling, wavelet numerical scheme, sub-grid modeling, image assimilation.

1. Introduction

The large scale analysis of complex fluid flows in domains ranging from climate sciences to engineering sciences requires to constitute dynamics models incorporating properly contributions that are difficult to specify precisely at the envisaged resolution scale. This includes for instance physical phenomena generating a forcing at small scale or the action of boundary layers, but also partially known inlet or boundary conditions, and eventually numerical errors arising from truncation policy and scale coarsening procedures. An accurate deterministic modeling of the effects of these processes is obviously hardly achievable in complex situations and we advocate instead the use of a stochastic modeling. Within this prospect, we aim at describing these missing contributions as random variables that will be referred to as flow uncertainties in the following. The modeling of such uncertainties but also of their evolution along time is of the utmost importance in ensemble methods used in geophysics, either for data assimilation or forecasting issues. In both cases, a modeling of the flow dynamics errors enables to rank the quality of some flow configurations. This authorizes ideally to set up efficient filtering strategies in which high errors are corrected by more meaningful data.

These errors or uncertainties are meant to represent principally small-scale physical processes ignored at the resolution scale. They include small-scales eddies, topographic forcing or boundary layers turbulence for instance and are responsible both of an energy dissipation but also of local backscatters of energy. The introduction of random variables constitutes an appealing mechanism to model inverse energy cascade mechanism [**24, 29, 36**], in so far as they enable a phenomenological modeling of the uncertainties involved. Recently those models have regained a great interest for the modeling of geophysical flows [**28, 37**] in climate sciences (see also the thematic issue [**33**]). In fluid mechanics, Large eddies simulations (LES) and Reynolds average simulations (RANS) face also the very same question: how to model the action on the resolved component of the small scales of the flow. Numerous turbulence modeling used in the aforementioned methodologies rely on eddies viscosity concept to model the energy dissipation due to unresolved scales. Eddy viscosity concept dates back to the work of Boussinesq [**3**] and Prandl mixing length [**34**]. It relies on the hypothesis that the energy transfer from the resolved scales to the subgrid scales can be described in a similar way as the molecular viscosity mechanism. It is therefore not at all related to any uncertainty or error quantities. In models dealing explicitly with a probabilistic modeling of the small scales there is thus some incoherency in representing the dissipative mechanism attached to random component through an eddy viscosity assumption. In this work we will not make use on such hypothesis. Instead, we will rely on an expression of the subgrid stress tensor that explicitly depends on the uncertainty variance.

This subgrid model is properly derived from a general stochastic model of the fluid motion in which the fluid parcels displacement is decomposed in two components: a smooth differentiable function and an uncertainty function uncorrelated in time but correlated in space [**31**]. The whole displacement field is defined as an Eulerian description of the form:

$$\boldsymbol{U}(\boldsymbol{x},t) = \boldsymbol{w}(\boldsymbol{x},t)dt + \boldsymbol{\sigma}(\boldsymbol{x},t)d\tilde{\boldsymbol{B}}_t. \tag{1}$$

In this expression, $\boldsymbol{w} = (w_1, w_2, w_3)$, corresponds to the smooth resolved velocity component of the flow referred to as the *drift* or resolved component. It is assumed

to be a deterministic differentiable function. The second component is a random component encoding the uncertainties we have on the flow. This uncertainty component, which is not differentiable in time, involves a diffusion tensor that has to be properly specified. Compared to the smooth drift, this component lives at a much smaller time scale. It is nevertheless defined at all the spatial scales. This approach is also close, in spirit, to the separation in term of a "coherent" component plus noise operated through adaptive wavelet basis [**8, 9**]. However, contrary to this approach relying on a Galerkin projection with an adaptive scale thresholding, our decomposition makes appear a diffusion tensor assembling the action of the unresolved uncertainty component on the resolved component.

This diffusion tensor can be specified explicitly as temporal or spatial correlation of the resolved component, see [**14**]. Another approach explored in this work consists to use the beforehand knowledge on the velocity field to optimally set up the effects of the unresolved uncertainty component through a data assimilation procedure.

The random field $\boldsymbol{U}(\boldsymbol{x}, t)$, is assumed to follow a stochastic linear momentum conservation principle that is mainly derived from a stochastic version of the Reynolds transport theorem. This modified transport theorem is presented in the following section.

The paper is organized as follow. After a brief presentation of the stochastic Navier-Stokes system devised in [**31**] in section 2, we describe a particular numerical scheme based on divergence free wavelets [**15, 16**]. This particular type of wavelets method together with the semi-implicit Euler scheme used to set up the discrete scheme are briefly presented in section 3. Therefore, we analyse the stability of this numerical scheme and give detail for the associated spatial discretization. Section 4 recalls the principle of variational data assimilation method for the discret model and numerical results in two space dimension in the case of an inhomogeneous turbulent flow are provided in section 6.

2. Navier-Stokes equation under uncertainty

As the system of Navier-Stokes equations we consider incorporates random uncertainties to describe unknown forcing or scale coarsening approximations, they constitute in essence a stochastic evolution system. Numerous methodological choices can be envisaged to constitute such a system. It is possible for instance to consider additional random forcing to a system of equations whose structure ensues from a deterministic formalization. This is the choice that has been the most often done since the work of Benssoussan [**2**]. Another choice, in the wake of Kraichnan's work [**17**], consists to close the large-scale representation in the Fourier space by relying on a Langevin stochastic representation [**19, 21, 23**]. Obviously the frontiers between these two methodologies are sometimes fuzzy, and numerous works rely on both of these strategies in order to setup the shape that should take the random variables evolution law [**21, 36**].

In this work, we shall rely on a different strategy that consists in directly defining the uncertainty as a location uncertainty on the resolution grid. A fluid particle location will be here defined only up to a Gaussian random field. The Navier-Stokes equations are then deduced from acceleration and second Newton's

principle. In a similar way as for the deterministic case, the main methodological tool used here is a stochastic version of the Reynolds transport theorem.

2.1. Stochastic Reynolds transport theorem. The Reynolds transport theorem provides the expression of the rate of change of a scalar function q within a material volume $\mathcal{V}(t)$ transported by the flow. Its extension to stochastic flows is given as [**31**]:

$$d\int_{\mathcal{V}(t)} q(\boldsymbol{x},t)d\boldsymbol{x} = \int_{\mathcal{V}(t)} \{dq_t + [\boldsymbol{\nabla}\cdot(q\boldsymbol{w}) + \frac{1}{2}\|\boldsymbol{\nabla}\cdot\boldsymbol{\sigma}\|^2 q - \sum_{i,j}\frac{1}{2}\frac{\partial^2}{\partial x_i \partial x_j}(a_{ij}q)_{|\boldsymbol{\nabla}\cdot\boldsymbol{\sigma}=0}]dt + \boldsymbol{\nabla}\cdot(q\boldsymbol{\sigma}d\tilde{\boldsymbol{B}}_t)\}d\boldsymbol{x}. \tag{2}$$

In this expression the first term is a time increment at fixed coordinates, $\boldsymbol{x}$, of the scalar quantity q. Let us note that this function is random and is not differentiable in time. The randomness of function q is an essential point in the derivation of this theorem as it requires to use a generalized form of Ito calculus – the Ito-Wentzell formula – adapted to the differentiation of the composition of two stochastic processes [**20**]. The last random term is built from a tempered representation of a Brownian map noted in a formal way through a convolution product $d\tilde{\boldsymbol{B}}_t = d\boldsymbol{B}_t \star \varphi_\nu$ and, $\boldsymbol{\sigma}_t$, a linear deterministic symmetric operator with null value outside the domain interior referred to as the diffusion tensor in the following. The random oscillating component is denoted:

$$\boldsymbol{\sigma}(\boldsymbol{x},t)d\tilde{\boldsymbol{B}}_t = \int \boldsymbol{\sigma}_t(\boldsymbol{x},\boldsymbol{y})d\tilde{\boldsymbol{B}}_t(\boldsymbol{y})d\boldsymbol{y}.$$

It is important to outline that an incompressibility condition on this component requires necessarily a divergence free diffusion tensor. The third term is related to the compression strength of the uncertainty field. The fourth term must be computed considering the diffusion tensor is divergence free. The tensor $\mathbf{a}(\boldsymbol{x})$ involved in this term is a matrix function associated to the diagonal elements of the covariance tensor. It corresponds hence to the uncertainty variance and is defined as:

$$a_{ij}(\boldsymbol{x},t) = \sum_k \sigma^\nu_{ik}(\boldsymbol{x},t)\sigma^\nu_{kj}(\boldsymbol{x},t), \tag{3}$$

where $\boldsymbol{\sigma}^\nu(\boldsymbol{x},\boldsymbol{y},t) = \boldsymbol{\sigma}(\boldsymbol{x},\bullet,t) \star \varphi_\nu(\boldsymbol{y})$ denotes a filtered version of the diffusion tensor along its second component. This rate of change formula is obtained from Ito-Wentzell differentiation of a function tending to the material volume characteristic function. The differentiation of the product of this characteristic function with the scalar function of interest, followed by a formal integration by part gives us the sought expression [**31**]. This relation allows us stating a mass conservation principle that accounts for the considered uncertainty on the fluid flow. Applying the previous transport theorem to the fluid density $\rho(\boldsymbol{x},t)$ and canceling this expression for arbitrary volumes, we get the following mass conservation constraint:

$$d\rho_t + \boldsymbol{\nabla}\cdot(\rho\boldsymbol{w})dt = \frac{1}{2}(\sum_{i,j}\frac{\partial^2}{\partial x_i\partial x_j}(a_{ij}\rho)_{|\boldsymbol{\nabla}\cdot\boldsymbol{\sigma}=0} - \frac{1}{2}\|\boldsymbol{\nabla}\cdot\boldsymbol{\sigma}\|^2\rho)dt - \boldsymbol{\nabla}\cdot(\rho\boldsymbol{\sigma}d\tilde{\boldsymbol{B}}_t). \tag{4}$$

For an incompressible fluid with constant density, canceling separately the slow deterministic terms and the rapid oscillating stochastic terms, and imposing to the

whole deformation field (1) to be volume preserving, this system simplifies in a set of incompressibility relations:

$$\boldsymbol{\nabla} \cdot (\boldsymbol{\sigma} d\tilde{\boldsymbol{B}}_t) = 0, \;\; \boldsymbol{\nabla} \cdot \boldsymbol{w} = 0, \;\; \boldsymbol{\nabla} \cdot (\boldsymbol{\nabla} \cdot \mathbf{a}) = 0, \tag{5}$$

composed of two standard volume preserving constraints accompanied with a less intuitive additional volume preserving constraint on the divergence of the uncertainty variance tensor. For divergence free homogeneous isotropic random fields such as the Kraichnan random field [**18**] this last constraint is naturally satisfied as those fields are associated to a constant diagonal variance tensor. In this case the system reduces hence to the standard divergence free constraint.

For isochoric flow with varying density we get a mass conservation constraint of the form:

$$d\rho_t + \boldsymbol{\nabla} \rho \boldsymbol{w} dt - \frac{1}{2} \sum_{i,j} \frac{\partial^2}{\partial x_i x_j} (\rho a_{ij}) dt = \boldsymbol{\nabla} \rho \sigma d\tilde{\boldsymbol{B}}_t. \tag{6}$$

In the case of the Kraichnan model the density variation involves a Laplacian diffusion and the density conditional expectation with respect to a given initial condition evolution comes to an intuitive advection diffusion equation. Let us note that the same kind of deterministic advection equation with an anisotropic diffusion is also obtained if the noise lies in the tangent plane of isodensity surfaces. This type of diffusion for the transport of a given scalar is often considered in geophysics to encode large scale mixing of stratified fluids. They are called isopycnal or isoneutral diffusion in this context [**12**,].

2.2. Linear momentum conservation. The mass conservation constraint and the stochastic version of the Reynolds theorem allows us expressing the balance between the momentum and the forces:

$$d \int_{\mathcal{V}(t)} \rho (\boldsymbol{w}(\boldsymbol{x}, t) dt + \boldsymbol{\sigma}(\boldsymbol{x}, t) d\tilde{\boldsymbol{B}}_t) d\boldsymbol{x} = \int_{\mathcal{V}(t)} \boldsymbol{F}(\boldsymbol{x}, t) d\boldsymbol{x}.$$

In this momentum equation, the differentiation in left hand term must be interpreted in a distribution sense (since the random term is non-differentiable). As for the forces in the right hand term, they are composed of standard deterministic forces such as the gravity force and forces acting on both the random and deterministic velocity components. For instance, the surface forces may be defined, as a direct extension of the deterministic, as:

$$\boldsymbol{\Sigma} = \int_{\mathcal{V}} -\boldsymbol{\nabla}(p dt + d\tilde{p}_t) + \mu(\Delta \boldsymbol{U} + \frac{1}{3} \boldsymbol{\nabla}(\boldsymbol{\nabla} \cdot \boldsymbol{U})).$$

In this expression μ is the dynamic viscosity, $p(\boldsymbol{x}, t)$ denotes the deterministic contribution of the pressure and $d\tilde{p}_t$ is a zero mean stochastic pressure fluctuation attached to the random component of the velocity. The Navier-Stokes equations under uncertainty are obtained incorporating the mass preservation principle (4) and requiring that on both sides the same mathematical structures stand [**31**]. For a constant density and for a general divergence free (incompressible) uncertainty

component, they read:

$$(\partial_t \boldsymbol{w} + \boldsymbol{w}\boldsymbol{\nabla}^T\boldsymbol{w} - \frac{1}{2}\sum_{i,j}\frac{\partial^2}{\partial x_i x_j}(a_{ij}\boldsymbol{w}))\rho = \rho\boldsymbol{g} - \boldsymbol{\nabla}p + \mu\Delta\boldsymbol{w}, \tag{7a}$$

$$\boldsymbol{\nabla}d\tilde{p}_t = -\boldsymbol{w}\boldsymbol{\nabla}^T\rho\boldsymbol{\sigma}d\tilde{\boldsymbol{B}}_t + \mu\Delta(\boldsymbol{\sigma}d\tilde{\boldsymbol{B}}_t), \tag{7b}$$

$$\boldsymbol{\nabla}\cdot(\boldsymbol{\sigma}d\tilde{\boldsymbol{B}}_t) = 0, \;\; \boldsymbol{\nabla}\cdot\boldsymbol{w} = 0, \;\; \boldsymbol{\nabla}\cdot(\boldsymbol{\nabla}\cdot\mathbf{a}) = 0. \tag{7c}$$

This system involves a first equation describing the evolution of the deterministic resolved component. It corresponds to the dynamics of the slow differentiable velocity component. Compared to the original Navier-Stokes formulation and similarly to the classical Reynolds decomposition, it includes an additional stress term that depends here on the resolved velocity component and on the uncertainty variance. The subsequent equations of this system denote a stochastic balance on the diffusion tensor and a mass conservation constraint respectively.

In the case of a divergence free isotropic model with constant density, we get a Navier-Stokes formulation with a constant eddy viscosity diffusivity coefficient :

$$(\frac{\partial\boldsymbol{w}}{\partial t} + \boldsymbol{w}\boldsymbol{\nabla}^T\boldsymbol{w} - \gamma\frac{1}{2}\Delta\boldsymbol{w})\rho = \rho\boldsymbol{g} - \boldsymbol{\nabla}p + \mu\Delta\boldsymbol{w}, \;\; \boldsymbol{\nabla}\cdot\boldsymbol{w} = 0, \tag{8}$$

where the diffusion is augmented by the noise variance. Note that in the previous non homogeneous model the diffusion term attached to the uncertainties cannot be directly related to the Boussinesq eddy viscosity formulation. However, it can be checked that for divergence free random field this term is globally dissipative as its energy is

$$\int_\Omega \boldsymbol{w}^T\sum_{i,j}\frac{\partial^2}{\partial x_i\partial x_j}(a_{ij}\boldsymbol{w})d\boldsymbol{x} = -\int_\Omega \|\nabla\boldsymbol{w}\|^2_{\mathbf{a}}d\boldsymbol{x}.$$

The subgrid stress tensor constitutes an anisotropic diffusion whose preferential directions of diffusion are given by the uncertainty variance. Setting the uncertainty diffusion tensor, $\boldsymbol{\sigma}$, or its variance tensor allows defining directly the subgrid diffusion term that has to be incorporated in the resolved drift component. For instance, considering uncertainties along iso-density surfaces provides immediately a clear justification of the isopycnal diffusion employed in oceanic circulation models [**31**]. The use also of constant eddy viscosity is also justified as the direct consequence of an isotropic homogeneous uncertainty component. Such an approach opens new perspectives for flow modeling that goes from *a priori* uncertainty specification to data based strategies. This framework, which does not rely neither on Reynolds averaging nor on spatial filtering concept, might be of great interest when uncertainties are prevalent as it is the case in geophysical flows or climate modeling. As another practical consequence, if one consider velocity fields supplied by particle image velocimetry methods, which are related to the true flow kinematics only up to a Gaussian uncertainty, then those measurements does not follow exactly the actual flow dynamics. Their physical interpretation should then be carried out with some care.

In the following we will experiment simple choices related in spirit to the scale similarity principles used to define subgrid stress tensor [**1**]. Before presenting the variance tensors we used, we present the numerical scheme we devised for the numerical simulation of the drift component.

3. A divergence-free wavelet numerical scheme for the drift component

The objective here is to construct a wavelet-based numerical discretization for the drift component equations of the stochastic system (7). Precisely, we consider the following system of an incompressible fluid:

$$(9)\quad \begin{cases} \frac{\partial \boldsymbol{w}}{\partial t} - \nu\Delta\boldsymbol{w} + \boldsymbol{w}\boldsymbol{\nabla}^T\boldsymbol{w} - \frac{1}{2}\sum_{i,j}\frac{\partial^2}{\partial x_i x_j}(a_{ij}\boldsymbol{w}) + \boldsymbol{\nabla}p = \boldsymbol{f},\ (\boldsymbol{x},t)\in\Omega\times]0,T[,\\ \boldsymbol{\nabla}\cdot\boldsymbol{w} = 0,\ \boldsymbol{x}\in\Omega,\\ \boldsymbol{w}(\boldsymbol{x},0) = \boldsymbol{w}_0,\ \boldsymbol{x}\in\Omega, \end{cases}$$

where $\Omega\subset\mathbb{R}^d$ is a *regular* open bounded subset satisfying periodic boundary conditions and $\nu = \mu/\rho$ denotes the kinematic viscosity. Since the matrix $\boldsymbol{a}(\boldsymbol{x},t)$ represents the covariance of the uncertainties on the flow, it is assumed to satisfy:

$$(10)\qquad \sum_{i,j} a_{ij}\xi_i\xi_j \geq \gamma|\xi|^2,\ \forall\ \xi\in\mathbb{R}^d,$$

with $\gamma > 0$ a positive constant. Let us suppose $\boldsymbol{w}$ to be a *regular* solution. Then, using integration by part and Poincaré's inequality, we get:

$$(11)\qquad \frac{1}{2}\frac{d}{dt}\int_\Omega|\boldsymbol{w}|^2 + \frac{\nu}{2}\int_\Omega|\boldsymbol{\nabla}\boldsymbol{w}|^2 + \frac{1}{2}\int_\Omega\|\nabla\boldsymbol{w}\|^2_{\mathbf{a}} \leq C\|\boldsymbol{f}\|^2_{H^{-1}(\Omega)^d}.$$

Again, using Poincaré for $\alpha > 0$, we have:

$$(12)\qquad \frac{d}{dt}\left(e^{\alpha t}\|\boldsymbol{w}\|^2_{L^2(\Omega)^d}\right) = e^{\alpha t}\left(\alpha\|\boldsymbol{w}\|^2_{L^2(\Omega)^d} + \frac{d}{dt}\|\boldsymbol{w}\|^2_{L^2(\Omega)^d}\right) \leq e^{\alpha t}\left(\frac{d}{dt}\|\boldsymbol{w}\|^2_{L^2(\Omega)^d} + \alpha C\int_\Omega|\boldsymbol{\nabla}\boldsymbol{w}|^2\right).$$

Thus, appropriately setting the value of α, we obtained:

$$(13)\qquad \|\boldsymbol{w}\|^2_{L^2(\Omega)^d} \leq e^{-\alpha t}\|\boldsymbol{w}_0\|^2_{L^2(\Omega)^d} + \int_0^t e^{\alpha(s-t)}\|\boldsymbol{f}\|_{H^{-1}(\Omega)^d}ds.$$

If there is no forcing term ($\boldsymbol{f} = 0$), from (11) and (13), we deduce that a *regular* solution $\boldsymbol{w}$ is uniformly bounded. Moreover, the energy of the solution decays exponentially in time:

$$(14)\qquad \|\boldsymbol{w}\|^2_{L^2(\Omega)^d} \leq C(\boldsymbol{w}_0) \text{ and } \|\boldsymbol{w}\|^2_{L^2(\Omega)^d} \leq e^{-\alpha t}C(\boldsymbol{w}_0).$$

To keep this stability condition, it is important for any numerical discretization associated to (9) to satisfy condition similar to (13) or (14). The objective of the forthcoming sections is to provide a wavelet-based numerical scheme of this type for the spatial discretization. The temporal discretization will rely on a finite difference method. Moreover, we will show that a semi-implicit Euler scheme combined to an explicit computation of the non linear term $\boldsymbol{w}\boldsymbol{\nabla}^T\boldsymbol{w}$ and the diffusion term $\frac{1}{2}\sum_{i,j}\frac{\partial^2}{\partial x_i x_j}(a_{ij}\boldsymbol{w})$ is stable under a particular CFL type condition. For convenience, we will first describ the spatial discretization and then, we will present the temporal scheme.

3.1. Spatial discretization. Galerkin type method is used to discretize in space the system (9). Since the velocity $\boldsymbol{w}$ is incompressible: $\nabla\cdot\boldsymbol{w} = 0$, to incorporate this constraint, a divergence-free wavelet basis is considered [**7, 15**]. Then, we suppose that the spatial domain is the hypercube $\Omega = [0,1]^d$. At a fixed spatial resolution $j > 0$, the approximated solution $\boldsymbol{w}_j$ is defined by its wavelet series:

$$(15)\quad \boldsymbol{w}_j(\boldsymbol{x},t) = \sum_{|\boldsymbol{j}|\leq j,\boldsymbol{k}\in\Lambda_j} \boldsymbol{d}_{\boldsymbol{j},\boldsymbol{k}}(t)\Psi^{\mathrm{div}}_{\boldsymbol{j},\boldsymbol{k}}(\boldsymbol{x}),\ \boldsymbol{\nabla}\cdot\Psi^{\mathrm{div}}_{\boldsymbol{j},\boldsymbol{k}} = 0,\ j\in\mathbb{N} \text{ and } \Lambda_j = [0,2^j-1]^d,$$

where $\{\Psi^{\text{div}}_{\boldsymbol{j},\boldsymbol{k}}\}_{\boldsymbol{j},\boldsymbol{k}\in\mathbb{Z}^d}$ is the divergence-free wavelet basis for the velocity function space. For details on the construction of a such wavelet basis, we refer the reader to [**7, 15**] and references therein.

Now, let us denote by $\mathbf{V}_j$ the multiresolution analysis spaces associated to the divergence-free wavelets basis $\{\Psi^{\text{div}}_{\boldsymbol{j},\boldsymbol{k}}\}_{\boldsymbol{j},\boldsymbol{k}\in\mathbb{Z}^d}$. It is known that supplemented with boundary conditions, $\mathbf{V}_j$ is a finite dimensional space [**7**], thus all the norm on $\mathbf{V}_j$ are equivalent. Particularly, we have:

$$\lim_{j\to+\infty}\|\boldsymbol{w}-\boldsymbol{w}_j\|_{L^2(\Omega)^d}=0 \text{ and } \|\boldsymbol{w}_j\|_{L^2(\Omega)^d}\lesssim\|\boldsymbol{w}\|_{L^2(\Omega)^d}.$$

One advantage of the wavelet basis is we have a direct and an inverse estimation on the solutions $\boldsymbol{w}_j$ and $\boldsymbol{w}$, very important in the proof of the stability of the numerical scheme. Precisely, we have Bernstein and Jackson type inequalities:

(16)
$$\|\boldsymbol{w}_j\|_{H^s(\Omega)^d}\lesssim 2^{js}\|\boldsymbol{w}_j\|_{L^2(\Omega)^d} \qquad \text{and} \qquad \inf_{\boldsymbol{w}_j\in\mathbf{V}_j}\|\boldsymbol{w}-\boldsymbol{w}_j\|_{L^2(\Omega)^d}\lesssim 2^{-js}\|\boldsymbol{w}\|_{H^s(\Omega)^d}.$$

In comparison to finite element method, the mesh size is $\delta x = 2^{-j}$, where $j > 0$ denotes the spatial resolution. We emphasise that the decomposition (15) provides a time and space scale separation and since the wavelet basis $\{\Psi^{\text{div}}_{\boldsymbol{j},\boldsymbol{k}}\}_{\boldsymbol{j},\boldsymbol{k}\in\mathbb{Z}^d}$ is explicitly defined, the unknowns are the wavelet coefficients $\boldsymbol{d}_{\boldsymbol{j},\boldsymbol{k}}(t)$. Then, to compute the coefficients $\boldsymbol{d}_{\boldsymbol{j},\boldsymbol{k}}(t)$ we must invert the mass and stiffness matrices of the wavelet basis $\{\Psi^{\text{div}}_{\boldsymbol{j},\boldsymbol{k}}\}_{\boldsymbol{j},\boldsymbol{k}\in\mathbb{Z}^d}$. This step will detailed in section 3.4 for the 2D case, the generalization to higher dimension is analogous.

3.2. Temporal discretization. The time discretization of (9) uses similar methods such as those proposed by [**7**]. For the sake of simplicity, we assume that $\boldsymbol{f} = 0$. Then, the projection of (7a) onto the divergence-free function space leads to:

$$\frac{\partial\boldsymbol{w}}{\partial t}-\nu\Delta\boldsymbol{w}=\mathbb{P}[-\boldsymbol{w}\boldsymbol{\nabla}^T\boldsymbol{w}+\frac{1}{2}\sum_{i,j}\frac{\partial^2}{\partial x_i x_j}(a_{ij}\boldsymbol{w})], \tag{17}$$

where $\mathbb{P}$ denotes the Leray projector: the orthogonal projector from $L^2(\Omega)^d$ onto the divergence-free function space $\mathcal{H}_{div}(\Omega)=\{\boldsymbol{u}\in L^2(\Omega)^d \ : \ \boldsymbol{\nabla}\cdot\boldsymbol{u}=0\}$. The projector $\mathbb{P}$ is in general explicitly defined in Fourier domain. In the present work, the computation of this projector is done though the projection onto the divergence-free wavelet basis $\{\Psi^{\text{div}}_{\boldsymbol{j},\boldsymbol{k}}\}$, see [**7, 15**].

Equation (17) can be seen as a heat equation with source term given by:

$$\mathbb{P}[-\boldsymbol{w}\boldsymbol{\nabla}^T\boldsymbol{w}+\frac{1}{2}\sum_{i,j}\frac{\partial^2}{\partial x_i x_j}(a_{ij}\boldsymbol{w})].$$

Hence, classical numerical schemes for the time discretization of the heat kernel can be used. Sticking to an implicit Euler scheme with a time step δt and setting $\boldsymbol{w}^n(\boldsymbol{x})\simeq\boldsymbol{w}_j(n\delta t,\boldsymbol{x})$ leads to:

$$(I-\nu\delta t\Delta)\boldsymbol{w}^{n+1}=\boldsymbol{w}^n-\delta t\mathbb{P}[\boldsymbol{w}^n\boldsymbol{\nabla}^T\boldsymbol{w}^n-\frac{1}{2}\sum_{i,j}\frac{\partial^2}{\partial x_i x_j}(a^n_{ij}\boldsymbol{w}^n)]. \tag{18}$$

In this case, the pressure p is recovered using the Helmholtz-Hodge decomposition:

$$\boldsymbol{w}\boldsymbol{\nabla}^T\boldsymbol{w} - \frac{1}{2}\sum_{i,j}\frac{\partial^2}{\partial x_i x_j}(a_{ij}\boldsymbol{w}) = \mathbb{P}[\boldsymbol{w}\boldsymbol{\nabla}^T\boldsymbol{w} - \frac{1}{2}\sum_{i,j}\frac{\partial^2}{\partial x_i x_j}(a_{ij}\boldsymbol{w})] - \nabla p.$$

The convergence and the computational efficiency of the discrete scheme (18) highly depends on the time step value. In the following section we establish a necessary stability condition for the method convergence. This condition will allow us to fix a maximal value for the time step in practice.

3.3. Stability of the semi-implicit Euler scheme. In this section, we will show that the semi-implicit Euler scheme (18) is stable in a specified meaning if the matrix $\boldsymbol{a}(\boldsymbol{x},t)$ is fixed and bounded on $\Omega\times[0,T]$:

$$\|\boldsymbol{a}\|_{L^\infty(\Omega\times[0,T])} \leq C \text{ and } \|\boldsymbol{\nabla}\cdot\boldsymbol{a}\|_{L^\infty(\Omega\times[0,T])} \leq C.$$

Precisely, we have the following proposition:

PROPOSITION 1.
If the kinematic viscosity ν, the anisotropic diffusion coefficients a_{ij}, the time step δt and the mesh size $\delta x = 2^{-j}$ satisfy:

$$\nu \geq \frac{1}{\sqrt{2}}\sqrt{\|\boldsymbol{a}\|_{L^\infty}^2 + C(\Omega)^2\|\boldsymbol{\nabla}\cdot\boldsymbol{a}\|_{L^\infty}^2} \qquad \text{and} \qquad \frac{\delta t}{\delta x^d} \leq C(\boldsymbol{w}^0,\boldsymbol{a},\nu), \tag{19}$$

then there exists $\lambda(\nu,\Omega) > 0$, a positive constant independent of δt and δx, such that the solution $\boldsymbol{w}^n$ of (18) is stable:

$$\|\boldsymbol{w}^{n+1}\|_{L^2(\Omega)^d}^2 \leq (1+\delta t\lambda(\nu,\Omega))^{-n}\|\boldsymbol{w}^0\|_{L^2(\Omega)^d}^2 + C_0\sum_{k=0}^{n-1}(1+\delta t\lambda(\nu,\Omega))^{k-n}, \tag{20}$$

where C_0 is a constant depending on ν, $\boldsymbol{w}^0$ and a_{ij}.

We infer that relation (20) is a discret version of (13). Then, a uniform bound for $\|\boldsymbol{w}^n\|_{L^2(\Omega)^d}^2$ can be deduced.

The prove of proposition 1 uses the following intermediate lemma:

LEMMA 1.
If the parameters ν, $\boldsymbol{a}$, δt and $\delta x = 2^{-j}$ satisfy the condition of (19), the solution $\boldsymbol{w}^n$ given by (18) remains bounded:

$$\|\boldsymbol{w}^n\|_{L^2(\Omega)^d}^2 \leq C(\boldsymbol{w}^0,\boldsymbol{a}),\ n = 0,\cdots,N \tag{21}$$

$$\delta t\sum_{k=1}^{N}\|\nabla\boldsymbol{w}^k\|_{L^2(\Omega)^{d\times d}}^2 \leq C(\boldsymbol{w}^0,\boldsymbol{a}). \tag{22}$$

where $C(\boldsymbol{w}^0,\boldsymbol{a}) > 0$ is a constant depending on the initial data.

Lemma 1 is analogous to lemma 5.3 of [**39**]. Very similar arguments can be used for its proof, this proof is provided in A. Let us now prove Proposition 1.

PROOF.
Taking $2\boldsymbol{w}^{n+1}$ as a test function in (18), for each term we obtain:

$$2\int_\Omega (1-\nu\delta t\Delta)\boldsymbol{w}^{n+1}\cdot\boldsymbol{w}^{n+1} - 2\int_\Omega \boldsymbol{w}^n\cdot\boldsymbol{w}^{n+1} =$$
$$\|\boldsymbol{w}^{n+1}\|^2_{L^2(\Omega)^d} - \|\boldsymbol{w}^n\|^2_{L^2(\Omega)^d} + 2\delta t\nu\|\nabla\boldsymbol{w}^{n+1}\|^2_{L^2(\Omega)^{d\times d}} + \|\boldsymbol{w}^{n+1}-\boldsymbol{w}^n\|^2_{L^2(\Omega)^d},$$

and due to the incompressibility constraint $\boldsymbol{\nabla}\cdot(\boldsymbol{\nabla}\cdot\boldsymbol{a})=0$, we have:

$$\frac{\partial^2}{\partial x_i\partial x_j}(a_{ij}\boldsymbol{w}^n) = \frac{\partial a_{ij}}{\partial x_j}\frac{\partial \boldsymbol{w}^n}{\partial x_i} + \frac{\partial}{\partial x_i}(a_{ij}\frac{\partial \boldsymbol{w}^n}{\partial x_j}).$$

Thus:

$$\begin{aligned}\int_\Omega \mathbb{P}[\frac{\partial^2}{\partial x_i\partial x_j}(a_{ij}\boldsymbol{w}^n)]\cdot\boldsymbol{w}^{n+1} &\leq \|\boldsymbol{a}\|_{L^\infty(\Omega\times[0,T])}\|\nabla\boldsymbol{w}^{n+1}\|_{L^2(\Omega)^{d\times d}}\|\nabla\boldsymbol{w}^n\|_{L^2(\Omega)^{d\times d}}\\ &+ \|\boldsymbol{\nabla}\cdot\boldsymbol{a}\|_{L^\infty(\Omega\times[0,T])}\|\boldsymbol{w}^n\|_{L^2(\Omega)^d}\|\nabla\boldsymbol{w}^{n+1}\|_{L^2(\Omega)^{d\times d}}.\end{aligned}$$

For the non linear term, since

$$\int_\Omega (\boldsymbol{w}^n\cdot\nabla)\boldsymbol{w}^n\cdot\boldsymbol{w}^n = -\frac{1}{2}\int_\Omega(\nabla\cdot\boldsymbol{w}^n)|\boldsymbol{w}^n|^2 = 0,$$

one obtains:

$$2\int_\Omega (\boldsymbol{w}^n\cdot\nabla)\boldsymbol{w}^n\cdot(\boldsymbol{w}^{n+1}-\boldsymbol{w}^n) \leq 2\|\boldsymbol{w}^n\|_{L^\infty(\Omega)^d}\|\nabla\boldsymbol{w}^n\|_{L^2(\Omega)^{d\times d}}\|\boldsymbol{w}^{n+1}-\boldsymbol{w}^n\|_{L^2(\Omega)^d}.$$

As we are in a finite dimensional space, in addition to (16), we have:

$$\|\boldsymbol{w}^n\|_{L^\infty(\Omega)^d} \leq 2^{jd/2}\|\boldsymbol{w}^n\|_{L^2(\Omega)^d}, \tag{23}$$

then, we get:

$$2\|\boldsymbol{w}^n\|_{L^\infty}\|\nabla\boldsymbol{w}^n\|_{L^2(\Omega)^d}\|\boldsymbol{w}^{n+1}-\boldsymbol{w}^n\|_{L^2(\Omega)^d} \leq 2.2^{jd/2}\|\boldsymbol{w}^n\|_{L^2(\Omega)^d}\|\nabla\boldsymbol{w}^n\|_{L^2(\Omega)^{d\times d}}\|\boldsymbol{w}^{n+1}-\boldsymbol{w}^n\|_{L^2(\Omega)^d}.$$

Gathering these estimations, we have:

$$\begin{aligned}&\|\boldsymbol{w}^{n+1}\|^2_{L^2(\Omega)^d} - \|\boldsymbol{w}^n\|^2_{L^2(\Omega)^d} + 2\delta t\nu\|\nabla\boldsymbol{w}^{n+1}\|^2_{L^2(\Omega)^{d\times d}} + \|\boldsymbol{w}^{n+1}-\boldsymbol{w}^n\|^2_{L^2(\Omega)^d}\\ &\leq 2\delta t 2^{\frac{jd}{2}}\|\boldsymbol{w}^n\|_{L^2(\Omega)^d}\|\nabla\boldsymbol{w}^n\|_{L^2(\Omega)^{d\times d}}\|\boldsymbol{w}^{n+1}-\boldsymbol{w}^n\|_{L^2(\Omega)^d} +\\ &\delta t\|\boldsymbol{a}\|_{L^\infty(\Omega\times[0,T])}\|\nabla\boldsymbol{w}^{n+1}\|_{L^2(\Omega)^{d\times d}}\|\nabla\boldsymbol{w}^n\|_{L^2(\Omega)^{d\times d}} + \delta t\|\boldsymbol{\nabla}\cdot\boldsymbol{a}\|_{L^\infty(\Omega\times[0,T])}\|\boldsymbol{w}^n\|_{L^2(\Omega)^d}\|\nabla\boldsymbol{w}^{n+1}\|_{L^2(\Omega)^{d\times d}}.\end{aligned}$$

Young's inequality leads to:

$$\begin{aligned}\|\boldsymbol{w}^{n+1}\|^2_{L^2(\Omega)^d} - \|\boldsymbol{w}^n\|^2_{L^2(\Omega)^d} + \delta t\nu\|\nabla\boldsymbol{w}^{n+1}\|^2_{L^2(\Omega)^{d\times d}} &\leq \delta t^2 2^{jd}\|\boldsymbol{w}^n\|^2_{L^2(\Omega)^d}\|\nabla\boldsymbol{w}^n\|^2_{L^2(\Omega)^{d\times d}}\\ &+ \frac{\delta t\|\boldsymbol{a}\|^2_{L^\infty(\Omega\times[0,T])}}{2\nu}\|\nabla\boldsymbol{w}^n\|^2_{L^2(\Omega)^{d\times d}}\\ &+ \frac{\delta t\|\boldsymbol{\nabla}\cdot\boldsymbol{a}\|^2_{L^\infty(\Omega\times[0,T])}}{2\nu}\|\boldsymbol{w}^n\|^2_{L^2(\Omega)^d}.\end{aligned} \tag{24}$$

Using Poincaré's inequality for the last term of (24), we deduce that:

$$\begin{aligned}\|\boldsymbol{w}^{n+1}\|^2_{L^2(\Omega)^d} - \|\boldsymbol{w}^n\|^2_{L^2(\Omega)^d} + \delta t\nu\|\nabla\boldsymbol{w}^{n+1}\|^2_{L^2(\Omega)^{d\times d}} &\leq \delta t^2 2^{jd}\|\boldsymbol{w}^n\|^2_{L^2(\Omega)^d}\|\nabla\boldsymbol{w}^n\|^2_{L^2(\Omega)^{d\times d}}\\ &+ \frac{\delta t\|\boldsymbol{a}\|^2_{L^\infty(\Omega\times[0,T])}}{2\nu}\|\nabla\boldsymbol{w}^n\|^2_{L^2(\Omega)^{d\times d}}\\ &+ \frac{\delta t C(\Omega)^2\|\boldsymbol{\nabla}\cdot\boldsymbol{a}\|^2_{L^\infty(\Omega\times[0,T])}}{2\nu}\|\nabla\boldsymbol{w}^n\|^2_{L^2(\Omega)^d}.\end{aligned} \tag{25}$$

Now let us define the constant $K(\boldsymbol{a},\nu)$ by:

$$K(\boldsymbol{a},\nu)=\frac{\|\boldsymbol{a}\|^2_{L^\infty(\Omega\times[0,T])}+C(\Omega)^2\|\boldsymbol{\nabla}\cdot\boldsymbol{a}\|^2_{L^\infty(\Omega\times[0,T])}}{2\nu}, \tag{26}$$

and fixed δt small enough such that:

$$\delta t 2^{jd}C(\boldsymbol{w}^0,\boldsymbol{a})\leq\frac{1}{2}(\nu-K(\boldsymbol{a},\nu))\Leftrightarrow\frac{\delta t}{\delta x^d}\leq\frac{(\nu-K(\boldsymbol{a},\nu))}{2C(\boldsymbol{w}^0,\boldsymbol{a})}=C(\boldsymbol{w}^0,\boldsymbol{a},\nu). \tag{27}$$

Since $\|\boldsymbol{w}^n\|^2_{L^2(\Omega)^d}\leq C(\boldsymbol{w}^0,\boldsymbol{a})$, by Lemma 1 and from (25) we deduce that:

$$\|\boldsymbol{w}^{n+1}\|^2_{L^2(\Omega)^d}-\|\boldsymbol{w}^n\|^2_{L^2(\Omega)^d}+\delta t\nu\|\nabla\boldsymbol{w}^{n+1}\|^2_{L^2(\Omega)^{d\times d}}\leq\frac{\delta t}{2}(\nu+K(\boldsymbol{a},\nu))\|\nabla\boldsymbol{w}^n\|^2_{L^2(\Omega)^{d\times d}}. \tag{28}$$

Again, using Poincaré's inequality, we get:

$$\|\boldsymbol{w}^{n+1}\|^2_{L^2(\Omega)^d}-\|\boldsymbol{w}^n\|^2_{L^2(\Omega)^d}+\frac{\delta t\nu}{C(\Omega)^2}\|\boldsymbol{w}^{n+1}\|^2_{L^2(\Omega)^d}\leq\frac{\delta t}{2}(\nu+K(\boldsymbol{a},\nu))\|\nabla\boldsymbol{w}^n\|^2_{L^2(\Omega)^{d\times d}}. \tag{29}$$

We set $\lambda(\nu,\Omega)=\frac{\nu}{C(\Omega)^2}$. Then, the sequence A_n defined by:

$$A_n=(1+\delta t\lambda(\nu,\Omega))^n\|\boldsymbol{w}^n\|^2_{L^2(\Omega)^{d\times d}}, \tag{30}$$

satisfies:

$$\begin{aligned}A_{n+1}-A_n &= (1+\delta t\lambda(\nu,\Omega))^n\left(\|\boldsymbol{w}^{n+1}\|^2_{L^2(\Omega)^d}-\|\boldsymbol{w}^n\|^2_{L^2(\Omega)^d}+\delta t\lambda(\nu,\Omega)\|\boldsymbol{w}^{n+1}\|^2_{L^2(\Omega)^d}\right)\\ &\leq (1+\delta t\lambda(\nu,\Omega))^n\frac{\delta t}{2}(\nu+K(\boldsymbol{a},\nu))\|\nabla\boldsymbol{w}^n\|^2_{L^2(\Omega)^{d\times d}}.\end{aligned}$$

Summation over n leads to:

$$A_n-A_0\leq\sum_{k=0}^{n-1}(1+\delta t\lambda(\nu,\Omega))^k\frac{\delta t}{2}(\nu+K(\boldsymbol{a},\nu))\|\nabla\boldsymbol{w}^k\|^2_{L^2(\Omega)^{d\times d}}.$$

Again, from Lemma 1 we have:

$$\delta t\|\nabla\boldsymbol{w}^n\|^2_{L^2(\Omega)^{d\times d}}\leq C(\boldsymbol{w}^0,\boldsymbol{a}),\ \forall\ n=0,1,\cdots,$$

thus:

$$A_n-A_0\leq C_0\sum_{k=0}^{n-1}(1+\delta t\lambda(\nu,\Omega))^k, \tag{31}$$

with $C_0=\frac{1}{2}(\nu+K(\boldsymbol{a},\nu))C(\boldsymbol{w}^0,\boldsymbol{a})$. Replacing A_n by its expression (30) ends the proof. □

To complete this section, we analyze now the behavior of the discretization error as δt goes to zero and $j>0$ goes to infinity:

$$\boldsymbol{e}^n=\boldsymbol{w}(\boldsymbol{x},t_n)-\boldsymbol{w}^n,$$

where $t_n=n\delta t$ denotes the corresponding discrete time and $\boldsymbol{w}(t,x)$ is the exact regular solution of (7a), which we suppose at least that $\boldsymbol{w}\in H^2(0,T;L^2(\Omega)^d)\cap\mathcal{C}^0(0,T;W^{1,+\infty}(\Omega)^d\cap H^1(\Omega)^d)$. Then, replacing $\boldsymbol{w}^n$ by $\boldsymbol{w}(\boldsymbol{x},t_n)$ in (18), we get:

$$\boldsymbol{w}(\boldsymbol{x},t_{n+1})-\boldsymbol{w}(\boldsymbol{x},t_n)-\nu\delta t\Delta\boldsymbol{w}(\boldsymbol{x},t_{n+1})+\delta t\mathbb{P}[(\boldsymbol{w}(\boldsymbol{x},t_n)\cdot\nabla)\boldsymbol{w}(\boldsymbol{x},t_n)-\frac{1}{2}\sum_{ij}\frac{\partial^2}{\partial x_i\partial x_j}(a_{ij}\boldsymbol{w}(\boldsymbol{x},t_n))]=\delta t\boldsymbol{\epsilon}^{n+1}. \tag{32}$$

where $\boldsymbol{\epsilon}^n$ denotes the consistency error. From (32), we infer that: $\boldsymbol{\epsilon}^n \in H^{-1}(\Omega)$ and it is divergence free: $\boldsymbol{\nabla} \cdot \boldsymbol{\epsilon}^n = 0$ and taking the difference of (32) and (18), reads:

(33)
$$\boldsymbol{e}^{n+1} - \boldsymbol{e}^n - \nu\delta t \Delta \boldsymbol{e}^{n+1} = \delta t \boldsymbol{\epsilon}^{n+1} - \delta t \mathbb{P}[(\boldsymbol{e}^n \cdot \nabla)\boldsymbol{w}(\boldsymbol{x}, t_n) + (\boldsymbol{w}^n \cdot \nabla)\boldsymbol{e}^n - \frac{1}{2}\sum_{ij} \frac{\partial^2}{\partial x_i \partial x_j}(a_{ij}\boldsymbol{e}^n)],$$

Thus, similar arguments to those used for the proof of Proposition 1 allow to show that:

$$\begin{aligned} \|\boldsymbol{e}^{n+1}\|^2_{L^2(\Omega)^d} - \|\boldsymbol{e}^n\|^2_{L^2(\Omega)^d} + \frac{\delta t \nu}{2}\|\nabla \boldsymbol{e}^{n+1}\|^2_{L^2(\Omega)^{d\times d}} &\leq \delta t K(\boldsymbol{a}, \nu)\|\nabla \boldsymbol{e}^n\|^2_{L^2(\Omega)^{d\times d}} \\ &+ \frac{4\delta t C^2(\Omega)}{\nu} 2^{jd}\|\boldsymbol{w}^n\|^2_{L^2(\Omega)^d}\|\nabla \boldsymbol{e}^n\|^2_{L^2(\Omega)^{d\times d}} \\ &+ \frac{4\delta t C^2(\Omega)}{\nu}\|\boldsymbol{e}^n\|^2_{L^2(\Omega)^d}\|\nabla \boldsymbol{w}(t_n)\|^2_{L^{+\infty}(\Omega)^{d\times d}} \\ &+ 2\delta t \|\boldsymbol{\epsilon}^{n+1}\|_{H^{-1}(\Omega)}\|\boldsymbol{e}^{n+1}\|_{L^2(\Omega)^d}. \end{aligned} \tag{34}$$

Otherwise, using (18), we get:

(35)
$$-\nu\Delta \boldsymbol{w}(\boldsymbol{x}, t_{n+1}) = -\partial_t \boldsymbol{w}(t_{\boldsymbol{x},n+1}) - \mathbb{P}[(\boldsymbol{w}(\boldsymbol{x}, t_{n+1})\cdot\nabla)\boldsymbol{w}(\boldsymbol{x}, t_{n+1}) - \frac{1}{2}\sum_{ij}\frac{\partial^2}{\partial x_i \partial x_j}(a_{ij}\boldsymbol{w}(\boldsymbol{x}, t_{n+1}))],$$

and

$$\begin{aligned} \boldsymbol{\epsilon}^{n+1} = -\partial_t \boldsymbol{w}(\boldsymbol{x}, t_{n+1}) + \frac{\boldsymbol{w}(\boldsymbol{x}, t_{,n+1}) - \boldsymbol{w}(\boldsymbol{x}, t_n)}{\delta t} + \mathbb{P}[(\boldsymbol{w}(\boldsymbol{x}, t_n)\cdot\nabla)\boldsymbol{w}(\boldsymbol{x}, t_n) - (\boldsymbol{w}(\boldsymbol{x}, t_{n+1})\cdot\nabla)\boldsymbol{w}(\boldsymbol{x}, t_{n+1})] \\ - \frac{1}{2}\mathbb{P}[\sum_{ij}\frac{\partial^2}{\partial x_i \partial x_j}(a_{ij}(\boldsymbol{x}, t_n)\boldsymbol{w}(\boldsymbol{x}, t_n) - a_{ij}(\boldsymbol{x}, t_{n+1})\boldsymbol{w}(\boldsymbol{x}, t_{n+1}))]. \end{aligned}$$

Since we assume that $\boldsymbol{w}$ is regular enough, we have:

$$\begin{aligned} \boldsymbol{\epsilon}^{n+1} = \frac{1}{\delta t}\int_{t_n}^{t_{n+1}} (t - t_n)\partial_{tt}\boldsymbol{w}(\boldsymbol{x}, t)dt - \mathbb{P}\left[\int_{t_n}^{t_{n+1}} \partial_t[(\boldsymbol{w}(\boldsymbol{x}, t)\cdot\nabla)\boldsymbol{w}(t)]dt\right] \\ + \frac{1}{2}\sum_{ij}\mathbb{P}\left[\int_{t_n}^{t_{n+1}} \frac{\partial^2}{\partial x_i \partial x_j}(\partial_t[a_{ij}\boldsymbol{w}(\boldsymbol{x}, t)])dt\right], \end{aligned} \tag{36}$$

and this gives:

$$\begin{aligned} \delta t \sum_n \|\boldsymbol{\epsilon}^{n+1}\|^2_{H^{-1}(\Omega)} \leq \delta t^2 \|\partial_{tt}\boldsymbol{w}\|^2_{L^2(0,T;H^{-1}(\Omega))} + 3\delta t^2 \|\partial_t[(\boldsymbol{w}\cdot\nabla)\boldsymbol{w}]\|^2_{L^2(0,T;H^{-1}(\Omega))} \\ + \frac{3\delta t^2}{2}\|\frac{\partial^2}{\partial x_i \partial x_j}(\partial_t[a_{ij}\boldsymbol{w}])\|^2_{L^2(0,T;H^{-1}(\Omega))}, \end{aligned}$$

and by definition we have:

(37)
$$\|\boldsymbol{e}^n\|^2_{L^2(\Omega)^d} \leq 2\left(\|\boldsymbol{w}^n\|^2_{L^2(\Omega)^d} + \|\boldsymbol{w}(t_n)\|^2_{L^2(\Omega)^d}\right),\ \|\nabla \boldsymbol{e}^n\|^2_{L^2(\Omega)^2} \leq 2\left(\|\nabla \boldsymbol{w}^n\|^2_{L^2(\Omega)^{d\times d}} + \|\nabla \boldsymbol{w}(t_n)\|^2_{L^2(\Omega)^{d\times d}}\right).$$

From (34) and recalling that the right-hand terms of inequalities (37) are bounded by constants depending only on the initial data, there exists hence a suitable constant depending only on the initial data such that:

$$\|\boldsymbol{e}^{n+1}\|_{L^2}^2 - \|\boldsymbol{e}^{n}\|_{L^2}^2 + \frac{\delta t\nu}{4}\|\nabla \boldsymbol{e}^{n+1}\|_{L^2}^2 \leq (\delta t + \delta x^{d/2})C(\boldsymbol{w}^0, a_{ij}, \Omega). \tag{38}$$

Summation of (38) over n shows that:

$$\max_n \|\boldsymbol{e}^{n}\|_{L^2(\Omega)^d}^2 \xrightarrow[\delta t\to 0,\delta x\to 0]{} 0. \tag{39}$$

and hence the semi-implicit temporal numerical scheme (18) converges.

3.4. Practical computational details of the divergence free numerical scheme. This section gives details on the implementation of the divergence-free wavelet numerical scheme in the especial case of the two space dimension: $\Omega = [0,1]^2$. We start by giving a brief reminder on the construction of a divergence-free wavelet basis. To construct divergence-free wavelet in $(L^2(\Omega))^2$, one needs first to have two multi-resolution analyses of $L^2(0,1)$ generated by the spaces V_j^1 and V_j^0 linked by differentiation:

$$\frac{d}{dx}V_j^1 = V_j^0.$$

In this case, it can be shown [**25**] that the associated wavelet generators ψ^1 and ψ^0 satisfy: $(\psi^1)' = 4\psi^0$. Then, the divergence-free wavelet generator is constructed by taking the curl of the scalar wavelet $\psi^1 \otimes \psi^1$:

$$\Psi^{div} = \mathbf{curl}[\psi^1 \otimes \psi^1] = 4\begin{pmatrix} \psi^1 \otimes \psi^0 \\ -\psi^0 \otimes \psi^1 \end{pmatrix}. \tag{40}$$

This divergence-free wavelet is contained in the standard multi-resolution analysis of $(L^2(\Omega))^2$ constituted by $\mathbf{V}_j = (V_j^1 \otimes V_j^0) \times (V_j^0 \otimes V_j^1)$, it provides hence fast divergence-free wavelet transform, see [**7, 16**]. This fast transform allows us to compute the divergence-free wavelet coefficients of $\boldsymbol{w}^n = (w_1^n, w_2^n)$ from those of its decomposition on the wavelet basis associated to $\mathbf{V}_j$ and conversely:

$$w_1^n = \sum_{|\boldsymbol{j}|\leq j,\boldsymbol{k}} d_{\boldsymbol{j},\boldsymbol{k}}^{1,n}\psi_{j_1,k_1}^1 \otimes \psi_{j_2,k_2}^0 \text{ and } w_2^n = \sum_{|\boldsymbol{j}|\leq j,\boldsymbol{k}} d_{\boldsymbol{j},\boldsymbol{k}}^{2,n}\psi_{j_1,k_1}^0 \otimes \psi_{j_2,k_2}^1. \tag{41}$$

Moreover, in (18) to compute the coefficients of $\boldsymbol{w}^{n+1}$ from those of $\boldsymbol{w}^n$, one needs to invert the matrix corresponding to operator $(1 - \delta t\nu\Delta)$. To avoid computing this inverse at each time step, we use the method described in [**4**], which relies on the heat kernel operator factorization. This method is very close to the alternated direction implicit methods. Precisely, for a given $\alpha \in \mathbb{R}$, we have:

$$(1 - \alpha\Delta) \approx (1 - \alpha\frac{\partial^2}{\partial x^2})(1 - \alpha\frac{\partial^2}{\partial y^2}) + O(\alpha^2). \tag{42}$$

Thus, we only have to invert the matrix of the one dimension operator $(1 - \delta t\nu\frac{\partial^2}{\partial x^2})$, and this is done once before starting the time integration.

Now, taking $\psi_{j_1,k_1}^1 \otimes \psi_{j_2,k_2}^0$ and $\psi_{j_1,k_1}^0 \otimes \psi_{j_2,k_2}^1$ as test functions in (18), we get two linear systems on the wavelet coefficients matrices:

$$\mathcal{A}_{\delta t}^1[d_{\boldsymbol{j},\boldsymbol{k}}^{1,n+1}]\mathcal{A}_{\delta t}^0 = \mathcal{M}^1[d_{\boldsymbol{j},\boldsymbol{k}}^{1,n}]\mathcal{M}^0 + \delta t\mathcal{M}^1[f_{\boldsymbol{j},\boldsymbol{k}}^{1,n}]\mathcal{M}^0 \tag{43}$$

and

$$\mathcal{A}^0_{\delta t}[d^{2,n+1}_{\boldsymbol{j},\boldsymbol{k}}]\mathcal{A}^1_{\delta t} = \mathcal{M}^0[d^{2,n}_{\boldsymbol{j},\boldsymbol{k}}]\mathcal{M}^1 + \delta t\mathcal{M}^0[f^{2,n}_{\boldsymbol{j},\boldsymbol{k}}]\mathcal{M}^1, \tag{44}$$

where $\mathcal{A}^i_{\delta t}$ are the stiffness matrix of the operator $(1 - \delta t\nu\frac{\partial^2}{\partial x^2})$ on the basis of $\{V^i_j\}_{i=0,1}$ and $\mathcal{M}^i$ are the mass matrices. These matrices are computed by solving en eigenvalue problem, see [**16**] and references therein. The source term s$[f^{1,n}_{\boldsymbol{j},\boldsymbol{k}}]$ and $[f^{2,n}_{\boldsymbol{j},\boldsymbol{k}}]$ are the matrices of the wavelet coefficients of the orthogonal projection onto the divergence-free function space of the non linear term and the anisotropic diffusion term:

$$\boldsymbol{f}^n = -\mathbb{P}[(\boldsymbol{w}^n \cdot \nabla)\boldsymbol{w}^n - \frac{1}{2}\sum_{ij}\frac{\partial^2}{\partial x_i \partial x_j}(a_{ij}\boldsymbol{w}^n)], \tag{45}$$

where the spatial derivatives are computed using finite difference method at the grid points.

The whole resolution method can be summarized as follows. Starting from $\boldsymbol{w}^0(x) = \boldsymbol{w}(\boldsymbol{x}, 0)$, compute its wavelet coefficients $[d^{1,0}_{\boldsymbol{j},\boldsymbol{k}}]$ and $[d^{2,0}_{\boldsymbol{j},\boldsymbol{k}}]$ on $\mathbf{V}_j = (V^1_j \otimes V^0_j) \times (V^0_j \otimes V^1_j)$ and for $0 \leq n \leq N$, repeat

Step 1: Using finite difference method, compute the term

$$\tilde{\boldsymbol{f}}^n = -(\boldsymbol{w}^n \cdot \nabla)\boldsymbol{w}^n - \frac{1}{2}\sum_{ij}\frac{\partial^2}{\partial x_i \partial x_j}(a_{ij}\boldsymbol{w}^n)$$

Step 2: Compute the divergence-free wavelet coefficients $[d^{div,n}_{\boldsymbol{j},\boldsymbol{k}}] = \mathbb{P}(\tilde{\boldsymbol{f}}^n)$ by:

$$\mathcal{M}^1[\tilde{f}^{1,n}_{\boldsymbol{j},\boldsymbol{k}}]\tilde{\mathcal{A}}^0 - (\tilde{\mathcal{A}}^0)^T[\tilde{f}^{2,n}_{\boldsymbol{j},\boldsymbol{k}}]\mathcal{M}^1 = \mathcal{M}^1[d^{div,n}_{\boldsymbol{j},\boldsymbol{k}}]\mathcal{R}^1 + \mathcal{R}^1[d^{div,n}_{\boldsymbol{j},\boldsymbol{k}}]\mathcal{M}^1$$

where $\mathcal{R}^1$ is the stiffness matrix of wavelet basis $\{\psi^1_{j,k}\}$, its terms correspond to $\langle(\psi^d_{j,k})', (\psi^1_{j',k'})'\rangle$ and the terms of $\tilde{\mathcal{A}}^0$ correspond to $\langle\psi^0_{j,k}, (\psi^d_{j',k'})'\rangle$.

Step 3: Compute $[f^{1,n}_{\boldsymbol{j},\boldsymbol{k}}]$ and $[f^{2,n}_{\boldsymbol{j},\boldsymbol{k}}]$ from $[d^{div,n}_{\boldsymbol{j},\boldsymbol{k}}]$ using the change of basis between $\{(\psi^1_{\boldsymbol{j},\boldsymbol{k}})'\}$ and $\{\psi^0_{\boldsymbol{j},\boldsymbol{k}}\}$.

Step 4: Find $[d^{1,n+1}_{\boldsymbol{j},\boldsymbol{k}}]$ and $[d^{2,n+1}_{\boldsymbol{j},\boldsymbol{k}}]$ solution of

$$\mathcal{A}^1_{\delta t}[d^{1,n+1}_{\boldsymbol{j},\boldsymbol{k}}]\mathcal{A}^0_{\delta t} = \mathcal{M}^1[d^{1,n}_{\boldsymbol{j},\boldsymbol{k}}]\mathcal{M}^0 + \delta t\mathcal{M}^1\boldsymbol{f}^n_1\mathcal{M}^0$$

$$\mathcal{A}^0_{\delta t}[d^{2,n+1}_{\boldsymbol{j},\boldsymbol{k}}]\mathcal{A}^1_{\delta t} = \mathcal{M}^0[d^{2,n}_{\boldsymbol{j},\boldsymbol{k}}]\mathcal{M}^1 + \delta t\mathcal{M}^0\boldsymbol{f}^n_2\mathcal{M}^1$$

As the matrices $\mathcal{A}^1_{\delta t}$ and $\mathcal{A}^0_{\delta t}$ are inverted once for all before starting the algorithm, step 4 corresponds thus only to a matrix multiplication. Let J be the maximal space resolution considered, then the theoretical complexity of Step 4 is $O(2^{3J})$. Step 2 is solved with a preconditioned conjugate gradient method, then its theoretical complexity is $O(2^{3J})$ and step 3 is a change of basis, whose complexity is linear. We deduce that the theoretical complexity of the method is about $O(2^{3J})$.

In practice, this theoretical complexity can be improved using adaptive methods and coherent structure extraction methods, see [**5, 8, 9, 40**].

4. Variational data assimilation

In this section we summarize the principle of the variational data assimilation methods for the Navier-Stokes equations with uncertainties. We use a generic notation for the different inner products and associated norms; without loss of generality, we consider the discret framework where the evolution system is given by (18) supplemented with a source terme $\boldsymbol{f}$:

$$(I-\nu\delta t\Delta)\boldsymbol{w}^{n+1}=\boldsymbol{w}^n+\delta t\mathbb{P}[-\boldsymbol{w}^n\boldsymbol{\nabla}^\tau\boldsymbol{w}^n+\frac{1}{2}\sum_{i,j}\frac{\partial^2}{\partial x_i x_j}(a_{ij}^n\boldsymbol{w}^n)+\boldsymbol{f}]. \tag{46}$$

We suppose that (46) can be rewritten as:

$$\boldsymbol{w}^{n+1}=\mathbb{M}(\boldsymbol{w}^n,a_{ij}^n,\boldsymbol{f}), \tag{47}$$

where $\mathbb{M}$ is a non linear operator.

Basically, variational data assimilation methods aim at combining measured observations of the system $\boldsymbol{w}_{ob}^k$, $0\leq k\leq N$ with the dynamical model (47) in order to improve the estimation of some parameters. Usually this is done by minimizing an energy functional. In this study, the parameters that we are concerned are the initial condition $\boldsymbol{w}^0$, the source term $\boldsymbol{f}$ or the anisotropic diffusion coefficients a_{ij}. Accordingly, if the control is the initial condition, the energy functional will be

$$\mathcal{J}(\boldsymbol{w}^0)=\frac{1}{2}\sum_{k=0}^{N}\|\mathbb{H}(\boldsymbol{w}^k)-\boldsymbol{w}_{ob}^k\|^2\delta t+\frac{\alpha}{2}\|\boldsymbol{w}^0\|^2,$$

where $\mathbb{H}$ denotes here the observation operator that maps the space of the solutions $\boldsymbol{w}^k$ to the space of the observations $\boldsymbol{w}_{ob}^k$. If the control is the initial condition and the source term, the energy functional is:

$$\mathcal{J}(\boldsymbol{w}^0,\boldsymbol{f})=\frac{1}{2}\sum_{k=0}^{N}\|\mathbb{H}(\boldsymbol{w}^k)-\boldsymbol{w}_{ob}^k\|^2\delta t+\frac{\alpha}{2}\|\boldsymbol{w}^0\|^2+\frac{\beta}{2}\|\boldsymbol{f}\|^2,$$

and if the control is the initial condition, the source term and the anisotropic diffusion, the energy functional corresponds to:

$$\mathcal{J}(\boldsymbol{w}^0,\boldsymbol{a},\boldsymbol{f})=\frac{1}{2}\sum_{k=0}^{N}\|\mathbb{H}(\boldsymbol{w}^k)-\boldsymbol{w}_{ob}^k\|^2\delta t+\frac{\alpha}{2}\|\boldsymbol{w}^0\|^2+\frac{\beta}{2}\|\nabla\cdot(\nabla\cdot\boldsymbol{a})\|^2+\frac{\gamma}{2}\|\boldsymbol{f}\|^2.$$

The minimization of $\mathcal{J}$ is often done using a gradient descent method. For the sake of explanation, let us supposed that we have to control only the initial condition. Then, using directional derivative, it is easy to see that:

$$\langle\nabla\mathcal{J}(\boldsymbol{w}^0),\delta\boldsymbol{w}^0\rangle=\sum_{k=0}^{N}\langle\mathbb{H}(\boldsymbol{w}^k)-\boldsymbol{w}_{ob}^k,\nabla_{\boldsymbol{w}}\mathbb{H}(\boldsymbol{w}^k)\cdot\nabla_{\boldsymbol{w}^0}\boldsymbol{w}^k\delta\boldsymbol{w}^0\rangle\delta t+\alpha\langle\boldsymbol{w}^0,\delta\boldsymbol{w}^0\rangle$$

Then, the gradient of $\mathcal{J}$ is defined on all the domain Ω. Thus, it is of great interest to have an efficient numerical method for the computation of this gradient. We used

the adjoint method. Precisely, let us introduce the following langragiean function:

$$\mathcal{L}(\boldsymbol{w}^0, \lambda^{k+1}) = \mathcal{J}(\boldsymbol{w}^0) - \sum_{k=0}^{N-1} \langle \boldsymbol{w}^{k+1} - \mathbb{M}(\boldsymbol{w}^k, a_{ij}^k, \boldsymbol{f}), \lambda^{k+1} \rangle \tag{48}$$

Then, the problem of the minimization of $\mathcal{J}$ under the dynamical constraint (47) becomes a saddle point problem for the Lagrangian $\mathcal{L}$. The first-order optimality conditions lead respectively to the direct model (47) and to the following adjoint problem:

$$\lambda^{N+1} = 0 \qquad \text{and } \lambda^k - \nabla_{\boldsymbol{w}} \mathbb{M}^*(\boldsymbol{w}^k, a_{ij}^k, \boldsymbol{f}) \lambda^{k+1} = \delta t \nabla_{\boldsymbol{w}} \mathbb{H}^*(\boldsymbol{w}^k)(\mathbb{H}(\boldsymbol{w}^k) - \boldsymbol{w}_{ob}^k),\ 0 \leq k \leq N, \tag{49}$$

where the asterisk denotes the adjoint operator and a backward integration of this adjoint problem gives:

$$\frac{\partial \mathcal{L}}{\partial \boldsymbol{w}^0} = \alpha \boldsymbol{w}^0 + \lambda^0. \tag{50}$$

Remark that, if the λ^k are optimal, namely $\frac{\partial \mathcal{L}}{\partial \lambda^k} = 0$, it is easy to see that:

$$\frac{\partial \mathcal{L}}{\partial \boldsymbol{w}^0} = \nabla \mathcal{J}(\boldsymbol{w}^0). \tag{51}$$

This observation is used during the numerical computation of $\nabla \mathcal{J}$, to control the initial condition, the source term and the anisotropic diffusion of the proposed model in the next section, with image data observations.

5. Numerical results

To implement the model presented in section 2, the first step is to choose a viscosity tensor $\boldsymbol{a}$ that satisfies the incompressibility condition (5) and the ellipticity property (10). There are several choices. The simplest is to set $\boldsymbol{a}$ as a diagonal tensor: $a_{ij} = \mu \delta_{ij}$, with $\mu > 0$ a positive constant or $a_{ij} = \mu(\boldsymbol{x}, t)\delta_{ij}$, with $\mu > 0$ and $\Delta \mu = 0$. In this cases $\boldsymbol{a}$ is a Laplacian operator. The more general choice is

$$\boldsymbol{a} = \begin{pmatrix} \partial_{xy}^2 \chi & -\partial_{xx}^2 \chi \\ \partial_{yy}^2 \chi & -\partial_{xy}^2 \chi \end{pmatrix}, \tag{52}$$

where χ is a two variables regular function. By construction, this choice implies:

$$\nabla \cdot [\nabla \cdot \boldsymbol{a}] = 0.$$

However, to ensure (10), the ellipticity constraint must to be added in the optimization functional.

In this study, we choose the two simplest cases: $a_{ij} = c\delta_{ij}$ referred as case one and $a_{ij} = \mu(\boldsymbol{x}, t)\delta_{ij}$ referred as case two. The taken observation operator is the optical flow operator:

$$\mathbb{H}(\boldsymbol{w}^k) - \boldsymbol{w}_{ob}^k := I_1^k(\boldsymbol{x} + \delta t \boldsymbol{w}^k) - I_0^k(\boldsymbol{x}),\ 0 \leq k \leq N,$$

with I_1^k and I_0^k two successive images and under the luminance invariance hypothesis we have:

$$I_1^k(\boldsymbol{x} + \delta t \boldsymbol{w}^k) - I_0^k(\boldsymbol{x}) = 0,\ 0 \leq k \leq N.$$

We made the control over the initial condition $\boldsymbol{w}_0(\boldsymbol{x})$, the anisotropic diffusion coefficients $a_{ij}(\boldsymbol{x},t)$ and the source term $\boldsymbol{f}$. Then, the encoded functional to be minimized is:

$$\mathcal{J}(\boldsymbol{w}^0,\boldsymbol{a},\boldsymbol{f}) = \frac{1}{2}\sum_{k=1}^{N} \|I_1^k(\boldsymbol{x}+\delta t\boldsymbol{w}^k)-I_0^k(\boldsymbol{x})\|_{L^2}^2\delta t+\frac{\alpha}{2}\|\boldsymbol{w}^0\|_{L^2}^2+\frac{\beta}{2}\|\nabla\cdot(\nabla\cdot\boldsymbol{a})\|_{L^2}^2+\frac{\gamma}{2}\|\boldsymbol{f}\|_{L^2}^2.$$

Accordingly, the gradient of $\mathcal{J}$ is computed using the adjoint method as described in section 4 and we used a quasi-newton method for the optimization procedure, with MATLAB software.

To evaluate the accuracy of the approach, we work on a sequence of synthetic particle images moved by a simulated velocity field. The dynamic of the fluid flow is given by a direct numerical simulation of 2D incompressible Navier-Stokes equations at $Re = 3000$, using the vorticity conservation equation and the Lagrangian equation for non-heavy particles transported by the flow (simulation details can be found in [**13**]). Image size is 256×256 pixels and the pixel grey levels have been normalized; examples of input images $I_0(x)$ from PIV is displayed in Figure 1.

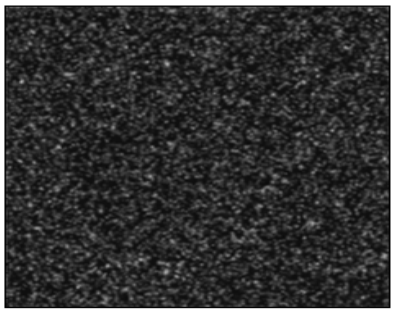

FIGURE 1. Example of used PIV image.

Estimated velocity and vorticity fields are evaluated based on the Root Mean Squared end-point Error (RMSE):

$$\text{RMSE} = \frac{1}{|\Omega|}\left(\sum_{\boldsymbol{x}\in\Omega}\left|\boldsymbol{w}(\boldsymbol{x})-\boldsymbol{w}_{\text{ref}}(\boldsymbol{x})\right|^2\right)^{\frac{1}{2}}.$$

Figure 2 shows the plot of this RMS error for both velocity field and its corresponding vorticity, where we took only five image sequences. The spatial resolution for the model is $j = 6$ while image resolution is $j = 8$. To interpolate the velocity field at the finer scales, we used the wavelet interpolation operator. Here we used the Daubechies wavelet generator with 10 vanishing moments.

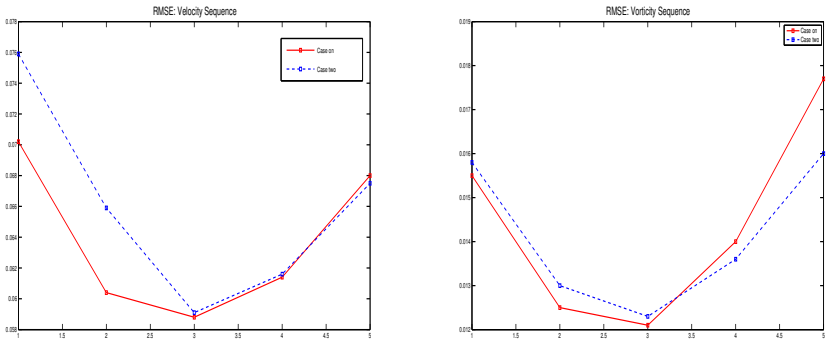

(a) RMSE on velocity (b) RMSE on vorticity

FIGURE 2. Velocity RMSE (left) and vorticity RMSE (right).

Figure 3 and Figure 4 show the plot of the total energy spectrum of the solution computed with our model, superimposed with that of the truth solution for the case two (case two includes the case one). As observed, the large scales have been well reproduced. This phenomena is also confirmed by the plots of the vorticity snapshots on Figures 5 and Figures 6, especially for $j = 6$. Moreover, we have a clear energy depreciation at fine scales for the proposed solution at $j = 7$, which is not the case for many classical large eddy simulation models [**14**].

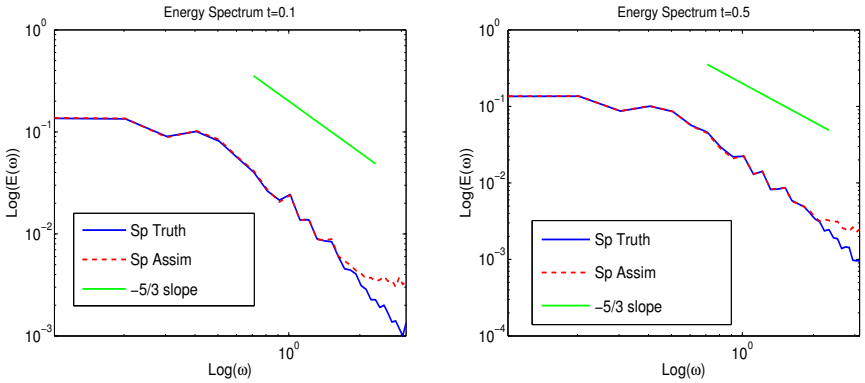

FIGURE 3. Total Energy Spectrum for the model at $j = 6$ (case two).

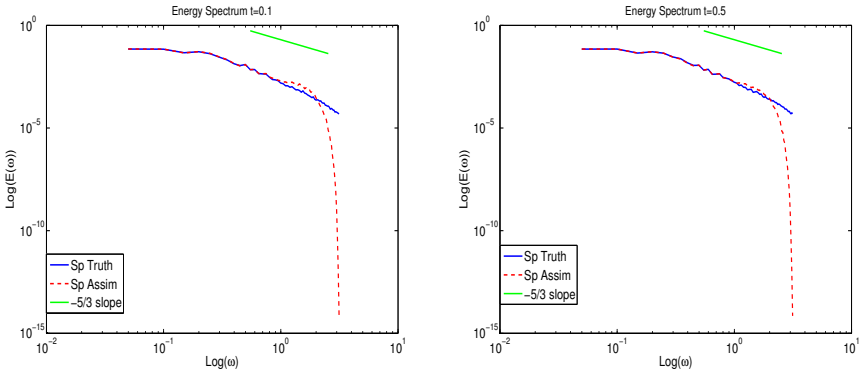

FIGURE 4. Total Energy Spectrum for the model at $j = 7$ (case two).

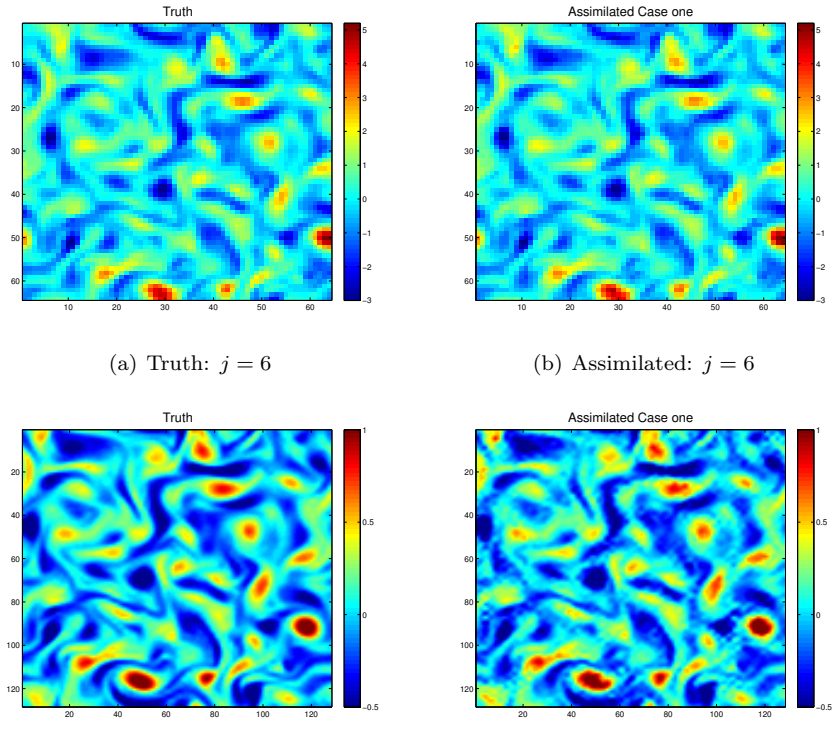

(a) Truth: $j = 6$

(b) Assimilated: $j = 6$

(c) Truth: $j = 7$

(d) Assimilated: $j = 7$

FIGURE 5. Vorticity snapshot plots for $j = 6$ top and $j = 7$ bottom (case one).

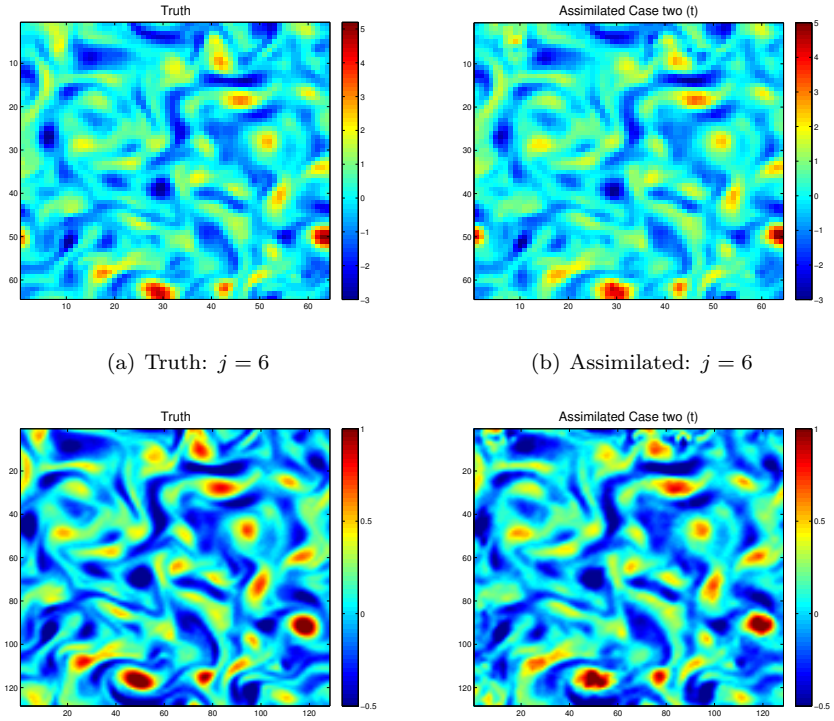

(a) Truth: $j = 6$ (b) Assimilated: $j = 6$

(c) Truth: $j = 7$ (d) Assimilated: $j = 7$

FIGURE 6. Vorticity snapshot plots for $j = 6$ top and $j = 7$ bottom (case two).

6. Conclusion

The present paper was devoted to image data assimilation in order to estimate a sub-grid viscosity model. The model was deduced under a stochastic uncertainty hypothesis on the flow. The main difficulty of the approach is the choice of the uncertainties covariance tensor. Tow simplest models was tested: a diagonal constant diffusion and an anisotropic diagonal diffusion. In each case, a simple divergence-free wavelet based numerical scheme was constructed and tested on synthetic particle image sequences in two space dimension. The results obtained are promising since they show a good large scale reproduction by the solution, especially for the total energy spectrum. Future works will deal with real data image sequences, with physical boundary conditions instead of periodic. In this case, it is well known that many turbulence models failed due to wall effect.

Appendix A. Proof of Lemma 1

To prove Lemma 1 it is sufficient to verify that if (27) holds, then by induction we must have:

$$\|\boldsymbol{w}^n\|_{L^2}^2 + \frac{\delta t}{2}(\nu - K(\boldsymbol{a}, \nu)) \sum_{k=1}^{n} \|\nabla \boldsymbol{w}^k\|_{L^2}^2 \leq C(\boldsymbol{w}^0, \boldsymbol{a}), \tag{53}$$

where $K(\boldsymbol{a},\nu)$ is defined in (26) and $C(\boldsymbol{w}^0,\boldsymbol{a})$ any constant such that:

$$C(\boldsymbol{w}^0,\boldsymbol{a}) \geq \|\boldsymbol{w}^0\|_{L^2}^2 + \delta t^2 2^{jd}\|\boldsymbol{w}^0\|_{L^2}^2\|\nabla\boldsymbol{w}^0\|_{L^2}^2 + \delta t K(\boldsymbol{a},\nu)\|\nabla\boldsymbol{w}^0\|_{L^2}^2. \tag{54}$$

Indeed, (25) gives this relation for $n=1$. Suppose (53) true for order $n-1$, then we have:

$$\delta t^2 2^{jd}\sum_{k=1}^{n-1}\|\boldsymbol{w}^k\|_{L^2}^2\|\nabla\boldsymbol{w}^k\|_{L^2}^2 \leq \delta t^2 2^{jd} C(\boldsymbol{w}^0,\boldsymbol{a})\sum_{k=1}^{n-1}\|\nabla\boldsymbol{w}^k\|_{L^2}^2, \tag{55}$$

and from (27) we get:

$$\delta t^2 2^{jd}\sum_{k=1}^{n-1}\|\boldsymbol{w}^k\|_{L^2}^2\|\nabla\boldsymbol{w}^k\|_{L^2}^2 \leq \frac{\delta t}{2}(\nu - K(\boldsymbol{a},\nu))\sum_{k=1}^{n}\|\nabla\boldsymbol{w}^k\|_{L^2}^2. \tag{56}$$

Otherwise, adding inequalities (25) for $k=1,\cdots,n$; reads:

$$\begin{aligned}&\|\boldsymbol{w}^n\|_{L^2}^2 + \delta t(\nu - K(\boldsymbol{a},\nu))\sum_{k=1}^{n}\|\nabla\boldsymbol{w}^k\|_{L^2}^2\\ &\leq C(\boldsymbol{w}^0,\boldsymbol{a}) + \delta t^2 2^{jd}\sum_{k=1}^{n-1}\|\boldsymbol{w}^k\|_{L^2}^2\|\nabla\boldsymbol{w}^k\|_{L^2}^2.\end{aligned} \tag{57}$$

Putting (56) in (57), we get the statements of (53) at order n and this proves Lemma 1.

References

[1] Bardina, J., Ferziger, J.H. & Reynolds W.C., Improved subgrid scale models for large eddy simulation, *AIAA*, **80**, 1357.

[2] Bensoussan, A. & Temam, R., 1973, Equations stochastique du type Navier-Stokes. *J. Funct. Anal.* **13**.

[3] Boussinesq, J., 1877, Essai sur la théorie des eaux courantes. Mémoires présentés par divers savants à l'Académie des Sciences, 23 (1): 1–680.

[4] Charton, P.& Perrier, V., 1996, A Pseudo-Wavelet Scheme for the Two-Dimensional Navier-Stokes Equations. *Comp. Appl. Math.* **15**,137–157.

[5] Cohen, A. 2003 *Numerical Analysis of Wavelet Methods*, Elsevier.

[6] Cottet, G.-H., Jiroveanu, D. & Michaux, B., 2003 ,Vorticity dynamics and turbulence models for large-eddy simulations. *M2AN* **37**, 187–207.

[7] Deriaz, E. & Perrier, V., 2006, Divergence-free and curl-free wavelets in 2D and 3D, application to turbulent flows. *J. of Turbulence* **7(3)**, 1–37.

[8] Farge, M., Pellegrino, G. & Schneider, K., 2001, Coherent vortex extraction in 3D turbulent flows using orthogonal wavelets. *Phys. Rev. Lett.* **87**, 054501.

[9] Farge, M., Schneider, K. & Kevlahan, N., 1999, Non-Gaussianity and coherent vortex simulation for two-dimensional turbulence using an adaptative orthogonal wavelet basis.*Phys. Fluids* **11**, 2187–2201.

[10] Flandoli, F., 2008, *SPDE in hydrodynamics*, *Lecture Notes in Math*, vol. 1942, chap. An intoduction to 3D stochastic Navier Stokes, 51–150. Berlin: Springer Verlag.

[11] Gawedzky, K. & Kupiainen, A., 1995, Anomalous scaling of the passive scalar. *Physical review letters* **75**, 3834–3837.

[12] Gent, P. & McWilliams, J., 1990, Isopycnal mixing in ocean circulation models. *J. Phys. Oceanogr.* **20**, 150–155.

[13] Heitz, D., Carlier, J. & Arroyo, G., 2007, Final report on the evaluation of the tasks of the workpackage 2, FLUID project deliverable 5.4. *Tech. rep.*, INRIA - Cemagref.

[14] Kadri Harouna, S. & Mémin, E., 2017, Stochastic representation of the Reynolds transport theorem: revisiting large-scale modeling. *Comp. and Fluids* **156**, 456–469.

[15] Kadri-Harouna, S. & Perrier, V., 2011, Helmholtz-Hodge Decomposition on $[0,1]^d$ by Divergence-free and Curl-free Wavelets. *J.-D Boissonat et (Eds), Curves and Surfaces, 2011, LNCS 6920, Springer Verlag Berlin Heidelberg*, 311–329.

[16] Kadri-Harouna, S. & Perrier, V., 2013, Effective construction of divergence-free wavelets on the square. *J. of Computational and Applied Math.* **240** 74–86.

[17] Kraichnan, R., 1959, The structure of isotropic turbulence at very high Reynolds numbers. *J. Fluid Mech.*, **5**, 477–543.

[18] Kraichnan, R.,1968, Small-scale structure of a randomly advected passive scalar. *Phys. Rev. Lett.* **11**, 945–963.

[19] Kraichnan, R., 1970, Small-scale structure of a randomly advected passive scalar. *Phys. Rev. Lett.* **11**, 945–963.

[20] Kunita, H., *Stochastic flows and stochastic differential equations*,1990, (Cambridge University Press), Cambridge, UK.

[21] Laval J.-P., Dubrulle, B.& McWilliams J.C., 2006, Langevin models of turbulence: Renormalization group, distant interaction algorithms or rapid distortion theory. *Phys. of Fluids*, **15(5)**, 1327-1339.

[22] Le Dimet, F.X. & Talagrand, O.,1986, Variational algorithms for analysis and assimilation of meteorological observations: theoretical aspects. *Tellus* **38A**, 97–110.

[23] Leith, C., 1971, Atmospheric predictability and two-dimensional turbulence. *J. Atmos. Sci.* 1971, **28**, 145–161.

[24] Leith, C., 1990, Stochastic backscatter in a subgrid-scale model: plane shear mixing layer. *Phys. of Fluids*, **2(3)**, 1521–1530.

[25] Lemarié-Rieusset, P. G., 1992, Analyses multi-résolutions non orthogonales, commutation entre projecteurs et dérivation et ondelettes vecteurs à divergence nulle. *Revista Matemática Iberoamericana* **8**, 221–236.

[26] Lilly, D., 1966, On the application of the eddy viscosity concept in the inertial subrange of turbulence. *Tech. Rep.* 123. NCAR.

[27] Majda, A. & Kramer, P., 1999, Simplified models for turbulent diffusion:theory, numerical modelling, and physical phenomena. *Physics report* **314**, 237–574.

[28] Majda, A., Timofeyev, I. and Vanden Eijnden, E., 1999, Models for stochastic climate prediction. *PNAS*, **96(26)**, 14687–14691.

[29] Mason, P.J. and Thomson, D.J., 1989, Stochastic backscatter in large-eddy simulations of boundary layers, *J. of Fluid Mech.,* **242**, 51–78.

[30] Melander, M., V. & Zabusky, N., 1989, Three Dimensional Vortex Tube Reconnection. Morphology for Orthogonal Offset Tubes. *Physica D,* 37.

[31] Mémin, E., 2014, Fluid flow dynamics under location uncertainty. *Geophysical & Astrophysical Fluid Dynamics* , http://hal.inria.fr/hal-00852874, in press.

[32] Mikulevicius, R. & Rozovskii, B.L., 2004, Stochastic Navier-Stokes equations for turbulent flows. *SIAM J. Math. Anal.* **35** (4), 1250–1310.

[33] Palmer, T. & Williams, P., 2008, Theme Issue 'Stochastic physics and climate modelling' *Phil. Trans. R. Soc.,* **366(1875)**.

[34] Prandtl, L., 1925, Bericht ÃŒber Untersuchungen zur ausgebildeten Turbulenz *Z. Angew. Math, Meth.***5**, 136-139..

[35] Sagaut, P., 2005, *Large-eddy simulation for incompressible flow - An introduction, third edition*. Springer-Verlag, Scientic Computation series.

[36] Schumann, U., 1995, Stochastic backscatter of turbulence energy and scalar variance by random subgrid-scale fluxes. *Proc. R. Soc. Lond. A* **451**, 293–318 .

[37] Slingo, J. and Palmer, T., 2011, Uncertainty in weather and climate prediction. *Phil. Trans. R. Soc.* A , **369**, 4751–4767.

[38] Smagorinsky, J., 1963, General circulation experiments with the primitive equation: I. the basic experiment. *Monthly Weather Review* **91**, 99–165.

[39] Temam, R., 1977, *Navier Stokes Equations*, North Holland, New York.

[40] Vasilyev, O.V., De Stefano, G., Goldstein, D. & Kevlahan, N. K.-R., 2008, Lagrangian dynamic SGS model for Stochastic Coherent Adaptive Large Eddy Simulation *J. Turbulence* **11**, 1-14.

Laboratoire Mathématiques, Image et Applications (MIA), Université de La Rochelle, Avenue Michel Crépeau 17042 La Rochelle, France
E-mail address: souleymane.kadri_harouna@univ-lr.fr

INRIA Rennes - IRMAR, Campus Universitaire de Beaulieu, 35042 Rennes cedex, France
E-mail address: etienne.memin@inria.fr